

Article

# Characterization and Curing Kinetics of Epoxy/Silica Nano-Hybrids

Cheng-Fu Yang<sup>1</sup>, Li-Fen Wang<sup>2</sup>, Song-Mao Wu<sup>3</sup> and Chean-Cheng Su<sup>1,\*</sup>

Received: 31 August 2015 ; Accepted: 10 October 2015 ; Published: 16 October 2015

Academic Editor: Teen-Hang Meen

<sup>1</sup> Department of Chemical and Materials Engineering, National University of Kaohsiung, No. 700, Kaohsiung University Rd., Nan-Tzu Dist., Kaohsiung 811, Taiwan; cfyang@nuk.edu.tw

<sup>2</sup> Department of Applied Chemistry and Materials Science, Fooyin University, 151 Jinxue Rd., Daliao Dist., Kaohsiung 831, Taiwan; sc112@fy.edu.tw

<sup>3</sup> Department of Electrical Engineering, National University of Kaohsiung, No. 700, Kaohsiung University Rd., Nan-Tzu Dist., Kaohsiung 811, Taiwan; sungmao@nuk.edu.tw

\* Correspondence: ccsu@nuk.edu.tw; Tel.: +886-7-591-9338; Fax: +886-7-591-9277

**Abstract:** The sol-gel technique was used to prepare epoxy/silica nano-hybrids. The thermal characteristics, curing kinetics and structure of epoxy/silica nano-hybrids were studied using differential scanning calorimetry (DSC), <sup>29</sup>Si nuclear magnetic resonance (NMR) and transmission electron microscopy (TEM). To improve the compatibility between the organic and inorganic phases, a coupling agent was used to modify the diglycidyl ether of bisphenol A (DGEBA) epoxy. The sol-gel technique enables the silica to be successfully incorporated into the network of the hybrids, increasing the thermal stability and improving the mechanical properties of the prepared epoxy/silica nano-hybrids. An autocatalytic mechanism of the epoxy/SiO<sub>2</sub> nanocomposites was observed. The low reaction rate of epoxy in the nanocomposites is caused by the steric hindrance in the network of hybrids that arises from the consuming of epoxide group in the network of hybrids by the silica. In the nanocomposites, the nano-scale silica particles had an average size of approximately 35 nm, and the particles were well dispersed in the epoxy matrix, according to the TEM images.

**Keywords:** sol-gel technique; nanocomposite; differential scanning calorimetry (DSC); autocatalytic mechanism

## 1. Introduction

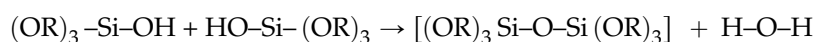
Epoxyes have many favorable properties such as high tensile strength and modulus, excellent chemical resistance, and high thermal stability. These characteristics make them ideal matrices for many applications, such as epoxy molding compounds (EMCs) [1], printed circuit boards (PCBs) [2], adhesives [3], paints [4], and high-performance composites [5]. Epoxy composites, which are hybrid organic-inorganic materials, have a wide range of engineering applications that require a high strength to weight ratio, low cost and ease of fabrication [6,7].

Sol gel-derived products have various applications, such as thin films [8,9], protective coatings [8], decorative coatings [10], electro-optic components [11] and composites [12]. Sol-gel methods are used to fabricate metal oxide from a chemical solution that acts as the precursor of an integrated network of either discrete particles or network polymers. Typical precursors are metal alkoxides and metal chlorides, which undergo various hydrolysis and polycondensation reactions [13,14]. An extensively studied alkoxide is tetraethyl orthosilicate (TEOS). Alkoxides are ideal chemical precursors for sol-gel synthesis because they react readily with water. The mechanism of the sol-gel process is as follows.

Hydrolysis:



Condensation:



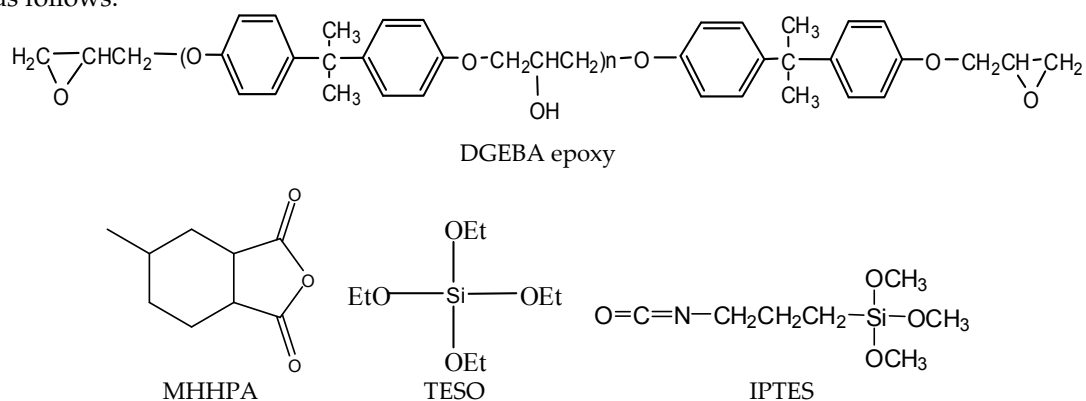
Polymerization is associated with the formation of a one-, two- or three-dimensional network of siloxane (Si–O–Si) bonds, accompanied by the formation of H–O–H and R–O–H species [15–19].

Epoxy/silica hybrids that comprise nanoparticles that are dispersed throughout an epoxy matrix have been widely studied because they exhibit a desired combination of the flexibility of epoxy and the hardness of silica nanoparticles [20,21]. The sol-gel process is an efficient means of preparing metal oxide networks at low temperatures. The structure of the inorganic material can be controlled by optimizing the synthetic conditions, including concentration, solvent/alkoxide ratio, temperature, pH, and the species of the catalyst and the solvent [22,23]. Whereas the curing kinetics and mechanisms of reaction of various epoxy resins have been studied using various methods, including infrared spectroscopy and differential scanning calorimetry. In fact, differential scanning calorimetry is more commonly used. The effects of nano-scale silica in epoxy resins on their curing kinetics have rarely been investigated. This study provides such critical information to elucidate the reactivity and to predict the curing behavior of epoxy/silica hybrids.

## 2. Experimental Section

### 2.1. Materials and Methods

The epoxy resin that is used in this work is the diglycidyl ether of bisphenol A (DGEBA) (shell 828, Shell Inc., Kawasaki, Japan). The epoxy resin was cured with 2,4-methylhexanhydrophthalic anhydride (MHHPA) (Shell Inc., Kawasaki, Japan). The alkoxides, 4,3-isocyanatopropyltriethoxysilane (IPTES) and tetraethoxysilane (TEOS), were purchased from Shin-Etsu Inc. (Naoetsu, Japan). The chemical structures of DGEBA, MHHPA, IPTES and TEOS are as follows.



A mixture of epoxy and IPTES, with an epoxy/IPTES weight ratio of 100/5, was stirred vigorously at 80 °C for 2 h to yield the silanized epoxy. Scheme 1 shows the preparation of silanized epoxy precursor. The silanized epoxy, TEOS, water, ethanol, and catalyst were mixed and stirred vigorously at room temperature for 1 h to obtain a homogeneous mixture. The amount of MHHPA that was required to provide an overall –COOH/epoxide molar ratio of 1/1 was then added to the mixture at room temperature and mixing was continued for another 5 min. The curing process was carried out at various temperatures to obtain cured epoxy/SiO<sub>2</sub> hybrids. Scheme 2 shows the process for preparation of epoxy/silica nano-hybrids.



using solid-state  $^{29}\text{Si}$  cross-polarization and magic angle spinning nuclear magnetic resonance spectroscopy. The morphology of epoxy/silica nanocomposites was analyzed by a transmission electron microscopy (TEM, model JEOL JEM 1200 EX, Tokyo, Japan) with an accelerating voltage of 100 kV.

### 3. Results and Discussion

#### 3.1. Characterization of Epoxy/Silica Nano-Hybrids

The chemical structure of silica in the epoxy/silica nanocomposites was examined using  $^{29}\text{Si}$  NMR. Figure 1 shows the solid-state  $^{29}\text{Si}$  NMR spectra of the epoxy/silica nanocomposite, which exhibited major chemical shifts at  $-91$  ppm,  $-102$  ppm, and  $-110$  ppm, which were attributed to silsesquioxane absorption by dihydroxy-substituted silica ( $\text{Q}^2$ ), monohydroxy-substituted silica ( $\text{Q}^3$ ) and nonhydroxy-substituted silica ( $\text{Q}^4$ ), respectively. These chemical shifts involved the Si–O–Si bonding of the silsesquioxane [24,25]. Scheme 3 shows the Q architecture of the polysilsesquioxane in the epoxy/silica nano-hybrids. Siloxane bridges in the silica, which were highly crosslinked in the epoxy/silica hybrid materials, were observed. Since the samples, having a  $\text{Q}^3$  and  $\text{Q}^4$  environment could be considered to include a highly condensed silica phase, the formation of the  $\text{SiO}_2$  network structure was complete in the prepared samples. The incomplete reaction of siloxane was not observed in the epoxy/silica nano-hybrids. Additionally, the amount of  $\text{Q}^4$  was observed to increase with TEOS content, indicating that a large amount of introduced TEOS may have promoted the formation of the silica network.

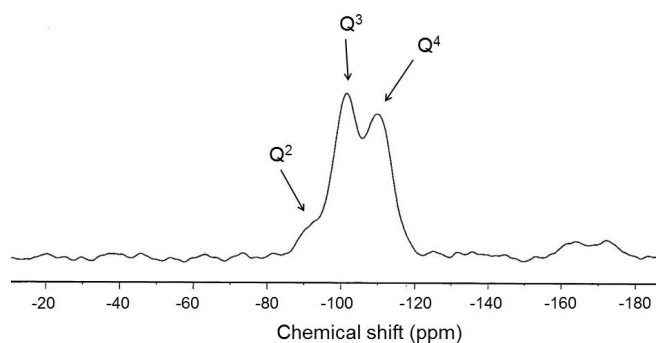
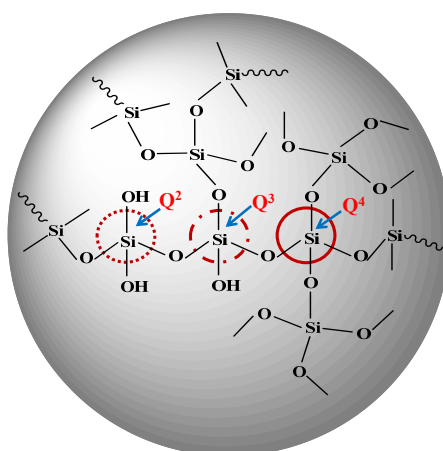


Figure 1. The solid-state  $^{29}\text{Si}$  NMR spectra of epoxy/silica nanocomposite.



Scheme 3. The Q structure of polysilsesquioxane.

### 3.2. Cure Kinetics of Epoxy/Silica Nano-Hybrids

A general equation for the autocatalytic curing reactions of many epoxy systems is as follows [7].

$$r = d\alpha/dt = (k_1 + k_2\alpha^m)(1 - \alpha)^n \quad (1)$$

where  $\alpha$  is the conversion;  $k_1$  and  $k_2$  are the apparent rate constants;  $r$  is the rate of the reaction, and  $m$  and  $n$  are the kinetic exponents of the reactions. The constant  $k_1$  in Equation (1) can be calculated if the initial reaction rate at  $\alpha = 0$  can be estimated. Kinetic constants  $k_1$  and  $k_2$  are assumed to be of the Arrhenius form:  $k_1 = A_1 \text{EXP}(-E_{a1}/RT)$  and  $k_2 = A_2 \text{EXP}(-E_{a2}/RT)$ , where  $A$  is the pre-exponential constant;  $E_a$  is the activation energy;  $R$  is the gas constant, and  $T$  is the absolute temperature.

The epoxy resin contained 10 phr (based on 100 parts of the epoxy) of silica and was cured at five isothermal temperatures of 100 °C, 110 °C, 120 °C, 130 °C, and 140 °C. Kinetic analysis was performed using the above kinetic models. Figure 2 plots the rate curves that were obtained at the five isothermal temperatures. These rate curves were distinctly autocatalytic, and the maximum rates were reached 5 min, 7 min, 11 min, 18 min, and 31 min after the start of the reaction at isothermal reaction temperatures of 100 °C, 110 °C, 120 °C, 130 °C, and 140 °C, respectively. The results in these figures also indicate that the presence of silica in the epoxy does not change its autocatalytic nature.

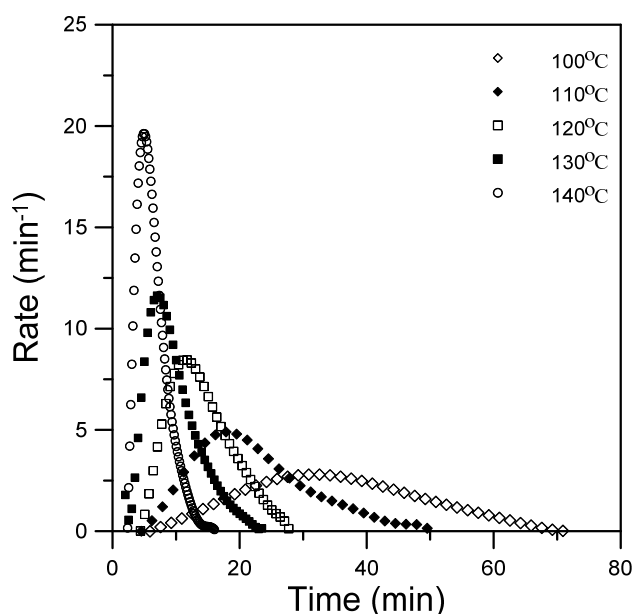


**Figure 2.** Plot of the reaction rate *vs.* time for epoxy/silica hybrids at five various temperatures.

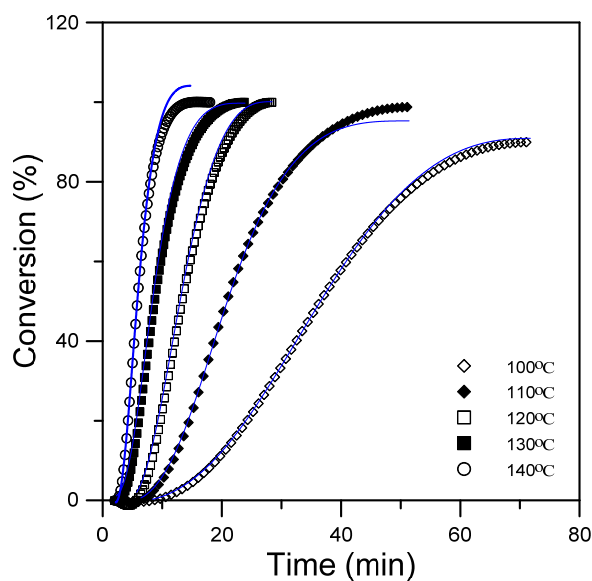
Table 1 presents the rate constants, which were obtained by iterative and graphic procedures. The orders of the reaction,  $m$  and  $n$ , were approximately 0.5 and 1.4, respectively, and their values did not vary much among the epoxy-silica hybrids. The value  $\Delta E_1$  and  $\Delta E_2$  for anhydride-cured DGEBA epoxy that were obtained in this study were  $80 \text{ kJmol}^{-1}$  and  $60 \text{ kJmol}^{-1}$ , respectively. The autocatalytic kinetic model and the obtained rate constants were used to calculate the empirical curves of conversions as a function of time for the epoxy/silica hybrids at five isothermal curing temperatures. Figure 3 shows that the empirical conversion curves fit the experimental data quite closely until the curing reactions had progressed to the point of vitrification. The model apparently describes the kinetics accurately, but diffusion control in the vitrified state limited the extent of the epoxy reactions.

Figure 4 plots the curves of rate *vs.* conversion for the epoxy-silica hybrids with 10 phr silica, which were cured at five isothermal temperatures. The conversion rate above which the curing rate

varied coincided with the formation of the gel point, at which the curing reaction of the gelled epoxy network began to slow down.

**Table 1.** Autocatalytic model constants for epoxy–silica hybrids.

$T$ (°C)	$m$	$n$	$k_1$ (min <sup>-1</sup> )	$k_2$ (min <sup>-1</sup> )	$E_{a1}$ (kJmol <sup>-1</sup> )	$E_{a2}$ (kJmol <sup>-1</sup> )	$A_1$	$A_2$
100	0.5	0.9	0.3	6.4	–	–	–	–
110	0.6	1.0	0.6	14.0	–	–	–	–
120	0.6	1.0	1.2	18.8	5.6	5.4	287	4699
130	0.6	1.0	1.6	30.0	–	–	–	–
140	0.6	0.9	1.9	45.2	–	–	–	–



**Figure 3.** Plot of the reaction rate vs. time for epoxy/silica hybrids at five various temperatures.

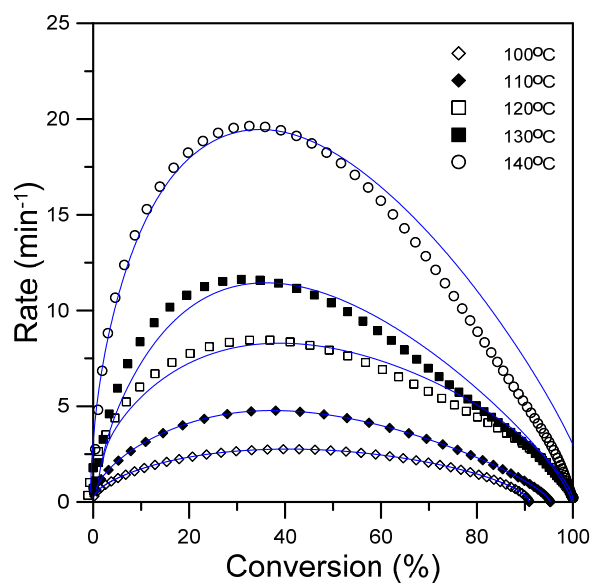


**Figure 4.** Plot of the reaction rate vs. conversion for epoxy/silica hybrids at five various temperatures.

### 3.3. Morphological Analysis

Figure 5 shows a TEM image of the silica/epoxy hybrid with 10 phr silica and the histogram of the particle sizes of silica that was cured at 140 °C for 60 min. TEM data reveal that the sizes of the nano-scale silica particles that were synthesized by the sol-gel method varied in the range 15–60 nm and the average size was 35 nm. In the epoxy/silica hybrid, nano-scale silica particles were dispersed uniformly throughout the epoxy matrix. This morphology reveals that 10% TEOS sufficed to form silica particles during the gel reaction. However, the amount of silica particles formed increased with the amount of charged TEOS. The sol-gel reaction changed the sizes of the nano-silica particles. The reactions involved various degrees of hydrolysis and condensation, yielding nano polysilsesquioxane particles of various sizes. Alkoxide addition to epoxy resins is thus expected to change not only their morphology but also the curing kinetics. Phase separation occurs and a heterogeneous morphology develops if the silica and the crosslinked epoxy are not miscible after curing. Additionally, phase morphology development during curing is expected to influence significantly the properties of the cured epoxy resins. Figure 6 show the silicon mapping of silica/epoxy hybrids with 10 phr silica. The silicon distribution mapping of the epoxy/silica hybrids revealed well mixed silicon, suggesting that the inorganic silica nano-particles in the epoxy/silica nanocomposites were distributed uniformly on the nanometer scale and their nano-architectures were well defined.

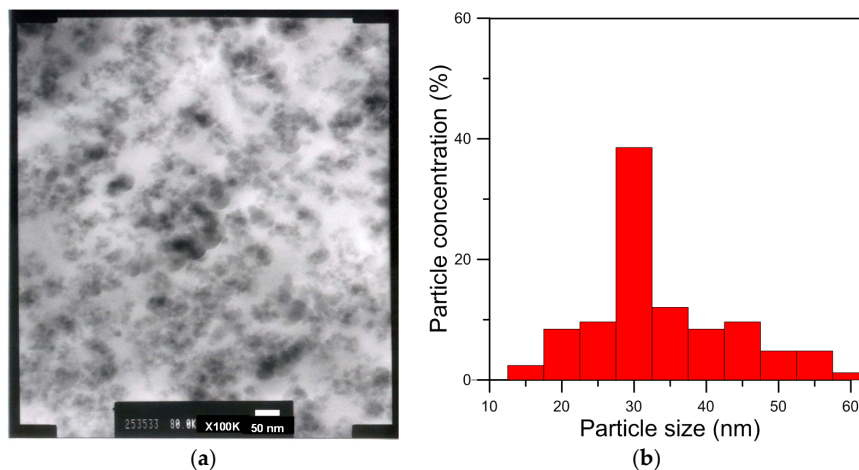


**Figure 5.** Transmission electron micrograph (TEM) of epoxy/silica hybrids with 10 phr silica: (a) TEM image and (b) the particle sizes distribution of silica.

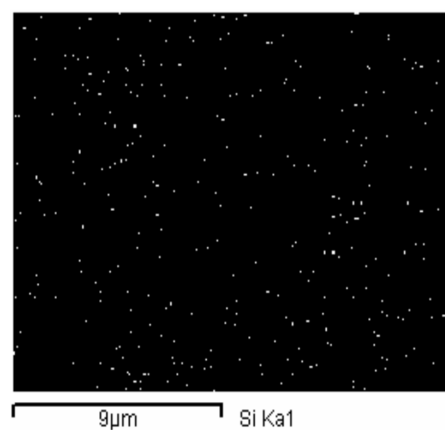


**Figure 6.** The silicon mapping of epoxy/silica hybrids with 10 phr silica.

#### 4. Conclusions

A new class of epoxy/silica nano-hybrids was prepared using a sol-gel technique. To improve the compatibility between the organic and inorganic phases, a coupling agent was used to modify the diglycidyl ether of bisphenol A (DGEBA) epoxy. Siloxane bridges in the silica, which were highly crosslinked in the epoxy/silica hybrid materials, were observed. The formation of the SiO<sub>2</sub> network structure in the prepared samples was complete. The difference in polarity between the inorganic and organic materials may have formed the nanophase-separated structure, which is shown in the TEM microphotographs. The sizes of the nano-scale silica particles in the nanocomposites varied in the range of 15–60 nm, averaging 35 nm, and the particles were well dispersed in the epoxy matrix, according to the TEM images. An autocatalytic mechanism of the curing of 10 phr epoxy/silica hybrids at various isothermal temperatures was observed. Kinetic parameters for the epoxy/silica hybrids were obtained and the proposed kinetic model was found to describe accurately the curing behavior of the epoxy/silica hybrids up to the vitrification point. A kinetic modeling approach is used to demonstrate how thermosetting epoxy resins that have been modified with silica behave during curing. The curing kinetics were corrected for the morphological development of the heterogeneous epoxy/silica hybrids during the curing progress.

**Acknowledgments:** This study is sponsored by the National Science Council of Taiwan under contract Nos. MOST 104-2221-E-390-025 and MOST 104-2622-E-390-003-CC3.

**Author Contributions:** The study was designed by Chean-Cheng Su. The data collection was performed by Cheng-Fu Yang, Li-Fen Wang and Song-Mao Wu. The data analysis was performed by Chean-Cheng Su. The overall planning was directed by Chean-Cheng Su.

**Conflicts of Interest:** The authors declare no conflict of interest.

#### References

1. Su, C.C.; Wei, C.H.; Yang, C.C. Elucidating How Advanced Organophosphine Accelerators Affect Molding Compounds. *Ind. Eng. Chem. Res.* **2013**, *52*, 2525–2536. [[CrossRef](#)]
2. Zhang, J.; Li, T.; Wang, H.P.; Liu, Y.; Yu, Y.F. Monitoring extent of curing and thermal-mechanical property study of printed circuit board substrates. *Microelectron. Reliab.* **2014**, *54*, 619–628. [[CrossRef](#)]
3. Sa, R.; Wei, Z.; Yan, Y.; Wang, L.; Wang, W.; Zhang, L.; Ning, N.; Tian, M. Catechol and epoxy functionalized ultrahigh molecular weight polyethylene (UHMWPE) fibers with improved surface activity and interfacial adhesion. *Compos. Sci. Technol.* **2015**, *113*, 54–62. [[CrossRef](#)]
4. Vakili, H.; Ramezanzadeh, B.; Amini, R. The corrosion performance and adhesion properties of the epoxy coating applied on the steel substrates treated by cerium-based conversion coatings. *Corros. Sci.* **2015**, *94*, 466–475. [[CrossRef](#)]
5. Ni, Y.; Chen, L.; Teng, K. Superior mechanical properties of epoxy composites reinforced by 3D interconnected graphene skeleton. *ACS Appl. Mater. Interfaces* **2015**, *7*, 11583–11591. [[CrossRef](#)] [[PubMed](#)]
6. Su, C.C.; Wei, C.H.; Li, B.C. Thermal and cure kinetics of epoxy molding compounds cured with thermal latency accelerators. *Adv. Mater. Sci. Eng.* **2013**, *391267*, 1–10. [[CrossRef](#)]
7. Su, C.C.; Woo, E.M. Cure kinetics and morphology of amine-cured tetraglycidyl-4,4'-diaminodiphenylmethane epoxy blends with polyetherimide. *Polymer* **1995**, *36*, 2883–2894. [[CrossRef](#)]
8. Catauro, M.; Bollino, F.; Papale, F.; Giovanardi, R.; Veronesi, P. Corrosion behavior and mechanical properties of bioactive sol-gel coatings on titanium implants. *Mater. Sci. Eng. C* **2014**, *43*, 375–382. [[CrossRef](#)] [[PubMed](#)]
9. Cao, D.; Zhang, Y.; Dong, W.; Yang, J.; Bai, W.; Chen, Y.; Wang, G.; Dong, X.; Tang, X. Structure, magnetic and transport properties of La<sub>0.7</sub>Ca<sub>0.3-x</sub>Sr<sub>x</sub>MnO<sub>3</sub> thin films by sol-gel method. *Ceram. Int.* **2015**, *1*, S381–S386. [[CrossRef](#)]
10. Subasri, R.; Madhav, C.S.; Somaraju, K.R.C.; Padmanabham, G. Decorative, hydrophobic sol-gel coatings densified using near-infrared radiation. *Surf. Coat. Technol.* **2012**, *206*, 2417–2421. [[CrossRef](#)]



11. Puja, G.; Manju, A. Dielectric relaxation and electro-optic response in nano-ceria dispersed ferroelectric liquid crystal nanocomposites: Effect of structural deformation and lattice straining. *RSC Adv.* **2015**, *5*, 29741–29747.
12. Wen, Z.L.; Xiao, P.; Li, Z.; Hong, W.; Luo, H.; Yu, X.Y.; Li, Y.; Chen, W.B. Microstructure and oxidation behavior of sol-gel mullite coating on SiC-coated carbon/carbon composites. *J. Eur. Ceram. Soc.* **2015**, *35*, 3789–3796.
13. Klein, L.C.; Garvey, G.J. Kinetics of the Sol-Gel Transition. *J. Non-Cryst. Solids* **1980**, *38*, 45–50. [[CrossRef](#)]
14. Brinker, C.J.; Keefer, K.D.; Schaefer, D.W.; Assink, R.A.; Kay, B.D.; Ashley, C.S. Sol-gel transition in simple silicates. *J. Non-Cryst. Solids* **1982**, *1*, 47–64. [[CrossRef](#)]
15. Yang, C.F.; Hsu, W.C.; Wu, S.M.; Su, C.C. Elucidating how surface functionalization of multiwalled carbon nanotube affects nanostructured MWCNT/titania hybrid materials. *J. Nanomater.* **2015**, *952797*, 1–8. [[CrossRef](#)]
16. Matijevic, E. Monodispersed colloids: Art and science. *Langmuir* **1986**, *2*, 12–20. [[CrossRef](#)]
17. Yoldas, B.E. Monolithic glass formation by chemical polymerization. *J. Mater. Sci.* **1979**, *14*, 1843–1949. [[CrossRef](#)]
18. Prochazka, S.; Klug, F.J. Infrared-transparent mullite ceramic. *J. Am. Ceram. Soc.* **1983**, *66*, 874–880. [[CrossRef](#)]
19. Ikesue, A.; Kinoshita, T.; Kamata, K.; Yoshida, K. Fabrication and optical properties of high-performance polycrystalline Nd:YAG ceramics for solid-state lasers. *J. Am. Ceram. Soc.* **1995**, *78*, 1033–1040. [[CrossRef](#)]
20. Ausman, K.D.; Piner, R.; Lourie, O.; Ruoff, R.S.; Korobov, M. Organic solvent dispersion of single-walled carbon nanotubes. *J. Phys. Chem. B* **2000**, *104*, 8911–8915. [[CrossRef](#)]
21. Afzal, A.; Siddiqi, H.M.; Saeed, S.; Ahmad, Z. Exploring resin viscosity effects in solventless processing of nano-SiO<sub>2</sub>/epoxy polymer hybrids. *RSC Adv.* **2013**, *3*, 3885–3892. [[CrossRef](#)]
22. Chen, Y.C.; Zhou, S.X.; Yang, H.H.; Wu, L.M. Structure and mechanical property of polyurethane/silica hybrid coatings. *Mol. Mater. Eng.* **2005**, *290*, 1001–1008. [[CrossRef](#)]
23. Afzal, A.; Siddiqi, H.M. A comprehensive study of the bicontinuous epoxy-silica hybrid polymers. *Polymer* **2011**, *52*, 1345–1355. [[CrossRef](#)]
24. Chiu, Y.C.; Liu, F.Y.; Maa, C.C.; Chou, I.C.; Riang, L.; Chiang, C.L.; Yang, J.C. Syntheses and characterization of novel P/Si polysilsesquioxanes/epoxy nanocomposites. *Thermochim. Acta* **2008**, *473*, 7–13. [[CrossRef](#)]
25. Liu, Y.L.; Su, Y.H.; Lai, J.Y. *In situ* crosslinking of chitosan and formation of chitosan-silica hybrid membranes with using  $\gamma$ -glycidoxypropyltrimethoxysilane as a crosslinking agent. *Polymer* **2004**, *45*, 6831–6837. [[CrossRef](#)]



© 2015 by the authors; licensee MDPI, Basel, Switzerland. This article is an open access article distributed under the terms and conditions of the Creative Commons by Attribution (CC-BY) license (<http://creativecommons.org/licenses/by/4.0/>).